

Permuted AdaIN: Enhancing the Representation of Local Cues in Image Classifiers

Oren Nuriel Sagie Benaim Lior Wolf
Tel Aviv University

Abstract

Recent work has shown that convolutional neural network classifiers overly rely on texture at the expense of shape cues, which adversely affects the classifier’s performance in shifted domains. In this work, we make a similar but different distinction between local image cues, including shape and texture, and global image statistics. We provide a method that enhances the representation of local cues in the hidden layers of image classifiers. Our method, called Permuted Adaptive Instance Normalization (pAdaIN), samples a random permutation π that rearranges the samples in a given batch. Adaptive Instance Normalization (AdaIN) is then applied between the activations of each (non-permuted) sample i and the corresponding activations of the sample $\pi(i)$, thus swapping statistics between the samples of the batch. Since the global image statistics are distorted, this swapping procedure causes the network to rely on the local image cues. By choosing the random permutation with probability p and the identity permutation otherwise, one can control the strength of this effect. With the correct choice of p , selected without considering the test data, our method consistently outperforms baseline methods in image classification, as well as in the setting of domain generalization.

1. Introduction

One of the early successes of computer vision was a face recognition system by Sakai et al., [25] that employed a simple neural network classifier. As it turns out, the network was relying on global image statistics, namely the average brightness, to perform recognition.

In this work, we demonstrate that removing the reliance on global image statistics improves classification results in modern networks. To mitigate the effect of the global statistics, a deliberate mismatch between the activations of a layer and its accumulated statistics is created. By normalizing with unmatched statistics, the distribution of activation values becomes unreliable as a source for label information.

Proper (undistorted) normalization is important. We, therefore, create the mismatch in the global statistics only

for a fraction of the images in the training set. However, this is enough to greatly reduce the reliance on global image information.

Our work is similar in spirit but different in conclusion from recent work that has identified a bias toward texture at the expense of shape. Such recent methods can often improve the performance of the image classifier on the test set and have been shown to dramatically increase the accuracy of the classifier on shifted image domains, in which image transformations change the image statistics but leave most of the shape unchanged.

In our work, we also show classification improvement as well as improvement in shifted domains. However, we demonstrate that the increase in classification performance occurs simultaneously for both category-based image recognition and texture recognition. This suggests that while the texture is often defined as local image statistics, becoming invariant to global image statistics improves both shape and texture recognition.

We demonstrate the effectiveness of our method in a number of settings. First, we demonstrate how classification performance improves when adding our permutation-based regularization. Second, we train a linear classifier on top of a pre-trained image-classification network’s representation layer and show that the accuracy of texture classification peaks exactly when the image classification results are maximized. Finally, we demonstrate the ability of our method to reduce the adverse effect of domain shift, by testing it in the setting of domain generalization and evaluating its robustness, when handling corrupted images.

2. Related Work

Bias towards texture A large body of work has shown that, unlike humans, networks tend to be biased towards textures in making decisions. Gatys et al., [10] have shown that training a linear classifier on top of a VGG19’s texture representation achieves similar performance to training VGG19 directly on this task. Geirhos et al., [11] observed this phenomenon in the context of pretrained ImageNet CNNs. They presented the ‘StylizedImageNet’ dataset, which is a version of ImageNet where the image style is altered, and show that

training with this dataset forces the network to learn a shape-based representation. Hermann and Kornblith [15] explored the factors that affect this bias, finding that while unsupervised training objectives and different factors have similar texture bias, adding augmentations leads to a significantly reduced texture bias. However, this resulted in a degradation in the network’s performance. Unlike these methods, from the technical perspective, our method does not rely on the additional supervision in the form of extended or modified datasets and instead directly modifies the architecture of the network. Our interpretation of the results is also different. We show that manipulating the global statistics, which are directly linked to style, does not hurt texture recognition. Therefore, we conclude that we do not steer the network away from recognizing texture.

Several contributions attempt to alleviate texture bias, by proposing an architectural change or a new training objective. Shi et al., [26] develop a Dropout-like algorithm which attempts to decorrelate the output of each layer with its less informative input regions. Wang et al., [28] penalize shallow layers for having predictive power, thus forcing the network to discard predictive signals, such as color and texture. Zhang and Zhu [33] show that adversarial training reduces texture bias. Carlucci et al., [4] propose to reduce texture bias by training the network to solve jigsaw puzzles. Unlike these methods, our method makes use of a novel normalization layer, which, as shown in Sec. 3.1, directly affects the dependence on global image statistics.

Normalization and style transfer Batch Norm [20] has become a standard mechanism for effectively training deep neural networks by normalizing activations by the statistics of the minibatch. To reduce minibatch dependencies, several alternatives were proposed, including Layer Normalization [2], Instance Normalization [27], and Group Normalization [29]. Our work utilizes the ability to swap the style statistics of images as part of a novel normalization layer. Unlike our normalization layer, its role is not to support efficient training, but to direct the network toward the desired emphasis on shape and fine details.

Instance norm by Ulyanov et al., [27], can be seen as a form of style normalization by normalizing feature statistics. Building on this view, Huang and Belongie [17] proposed Adaptive Instance Normalization (AdaIN) as a form of style transfer, by first normalizing the target image style statistics and then rescaling by source image style statistics. These style manipulation through normalization layer methods are mostly applied in the generative setting, where they can be used for texture synthesis and style transfer, while our method focuses on image recognition.

Our method builds upon AdaIN to swap the style statistics of different elements activation. As far as we are aware, while other methods use style transfer to construct an im-

proved dataset [15, 11] to alleviate the reliance on global image statistics, our method is the first to do so within a network architecture.

Concurrently with our work, anonymous authors have proposed a method called MIXSTYLE that is closely related [1]. Building upon the mixup method [32], this method mixes the statistics used for normalization between two samples using a convex combination determined by the *Beta* distribution. In our work, we apply a random permutation to replace statistics between all samples in a batch. This permutation varies between layers, causing the activations to be influenced by many of the samples in the batch. Instead of the parameter α of the *Beta* distribution, we control the strength of the effect more intuitively, by applying the process at probability p .

3. Method

We start with a short motivation, after which we describe the exact details of our method.

3.1. Motivation

To motivate our method, we conduct a simple experiment devised to visualize the effect of swapping statistics of intermediate layer representations. Consider a standard hourglass-like convolutional autoencoder trained with reconstruction loss on natural images from the Stanford Car Dataset [21]. Since an autoencoder is trained to reconstruct images, it is a natural candidate to visualize the effect of pAdaIN at different representation layers. We consider two image inputs, a and b and inspect the effect on the reconstruction of a , when swapping their statistics at different layers of the pretrained encoder. The decoder is left unchanged. As a comparison, we also consider the effect of transferring the style of image b to a using the method of Gatys et al., [10].

As can be see in Fig. 1, when pAdaIN is applied, the reconstructed image has similar global statistics, such as color and overall image appearance of b but the finer details of image a are preserved. Applying pAdaIN on more layers, results in a larger transfer of the global statistics of b . In contrast, when using style transfer, the fine details of a are borrowed from image b and are no longer preserved. For example in Fig. 1, when applying style transfer, the bird on a tree was given the fine details of the shark under water, and similarly a cat was given the texture of the elephant skin. However, our method did not transfer such fine details. We argue that preserving these fine details, while transferring the global ones, results in an improved classification accuracy, robustness to imaging conditions and generalization to new visual domains.

3.2. Adaptive Instance Normalization

We begin by defining Instance Normalization (IN), as formulated in [27] and [17]. For a given convolutional neural

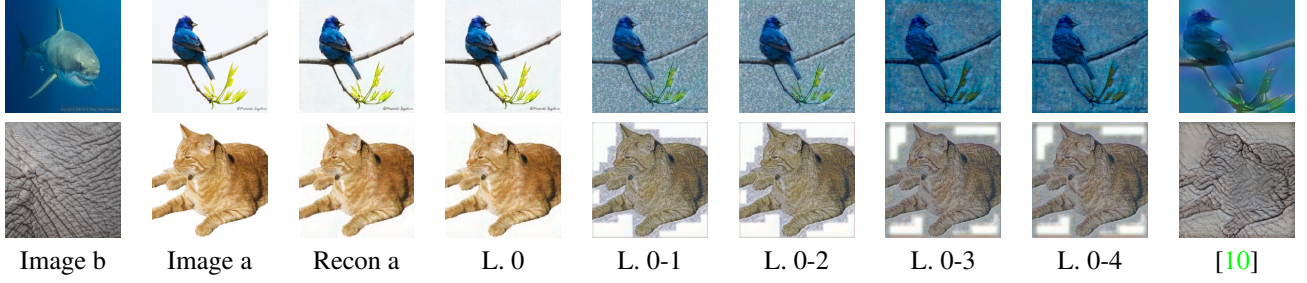


Figure 1. The result of applying pAdaIN on different layers of an encoder in a standard auto-encoder. The input image and reconstructed image are shown on the left. The reconstructed results when applying pAdaIN on different layers of the encoder are shown subsequently. The last image on the right is the result of applying style transfer using the method of Gatys et al., [10]. L.=layer; Recon=Reconstruction.

network, let the output activations of a given convolutional layer be $x \in \mathbb{R}^{N \times C \times H \times W}$, where N is the batch size, C the number of channels, H the height of the layer, and W its width. Instance Norm is then defined as:

$$\text{IN}(x) = \gamma \left(\frac{x - \mu(x)}{\sigma(x)} \right) + \beta \quad (1)$$

where $\mu(x)$ and $\sigma(x)$ both in $\mathbb{R}^{N \times C}$, are the mean and standard deviation, computed along the spatial dimensions (H and W) for each channel (c) and sample in the batch (n) independently:

$$\mu_{nc}(x) = \frac{1}{HW} \sum_{h=1}^H \sum_{w=1}^W x_{nchw} \quad (2)$$

$$\sigma_{nc}(x) = \sqrt{\frac{1}{HW} \sum_{h=1}^H \sum_{w=1}^W (x_{nchw} - \mu_{nc}(x))^2 + \epsilon} \quad (3)$$

γ and β , both in $\mathbb{R}^{N \times C}$, are the re-scaling affine parameters learned independently of x .

The above operation is applied in the same manner both at train and test time. As detailed in [17], IN can be viewed as normalizing the style statistics of each input in the batch. Adaptive Instance Normalization (AdaIN) builds upon this view by first normalizing the style statistics of an input a , thus extracting the content of b , and then scaling the normalized output by the statistics of a target style input b . This allows the transfer of style from a to b . Specifically, let $a, b \in \mathbb{R}^{C \times H \times W}$, then AdaIN is defined as:

$$\text{AdaIN}(a, b) = \sigma(b) \left(\frac{a - \mu(a)}{\sigma(a)} \right) + \mu(b) \quad (4)$$

where $\mu(x)$ and $\sigma(x)$ (resp. $\mu(y)$ and $\sigma(y)$) are the mean and standard deviation of x (resp. y) over its spatial dimension, computed for each channel.

3.3. Permuted AdaIN

Given an input activations $x \in \mathbb{R}^{N \times C \times H \times W}$, let $\pi(x) = [x_{\pi(1)}, x_{\pi(2)}, \dots, x_{\pi(N)}] \in \mathbb{R}^{N \times C \times H \times W}$ be the result of

applying a permutation π to the elements of a given mini-batch $x = x_1, \dots, x_N$ along the minibatch axis.

The result of applying pAdaIN on a single sample x_i in the context of its batch and for a given permutation π is given by

$$\text{p-IN}^\pi(x_i) = \text{AdaIN}(x_i, x_{\pi(i)}) \quad (5)$$

pAdaIN is then defined for the entire tensor x in size $\mathbb{R}^{N \times C \times H \times W}$ as:

$$\text{pAdaIN}(x) = \begin{cases} x, & \text{probability } p \\ (\text{p-IN}^\pi(x_1), \dots, \text{p-IN}^\pi(x_N)) & \text{otherwise} \end{cases}$$

where π is a uniformly chosen permutation, and p is a hyper-parameter fixed ahead of training. pAdaIN is only applied during training time and not at test time. We apply pAdaIN to the output activations of all convolutional layers and in particular, before applying batch normalization.

4. Experiments

Our experiments explore classification accuracy of both objects and texture, robustness to image corruption, and generalization to new domains.

4.1. Image Classification

We evaluate pAdaIN in the context of image classification on both CIFAR100 and ImageNet. To evaluate pAdaIN, for every architecture, we add a pAdaIN layer before every use of batch normalization and after using a convolutional layer.

For CIFAR100, we consider the architectures of PyramidNet [12], ResNet18 and ResNet50 [13]. During training, we apply a padding of 4, a random crop and a random rotation of up to 15%, resulting in images of size 32×32 . The networks are trained on a batch size of 128 with an SGD with Momentum optimizer with momentum of 0.9 and weight decay of $5e^{-4}$. We use 200 epochs, start training with a learning rate of 0.1 and divide the learning rate by 5 at epochs 60, 120 and 160.

For ImageNet, we consider the architectures of ResNet50, ResNet101 and ResNet152 [13]. We train for

Table 1. Top-1 accuracy for CIFAR100 on different architectures. pAdaIN is applied with $p = 0.01$.

METHOD	ARCHITECTURE	CIFAR 100
BASELINE	PYRAMIDNET	83.49
PADAIN	PYRAMIDNET	84.17
BASELINE	RESNET18	76.01
PADAIN	RESNET18	77.56
BASELINE	RESNET50	78.22
PADAIN	RESNET50	79.03

Table 2. Top-1 and Top-5 accuracy for ImageNet on different architectures. pAdaIN is applied with $p = 0.01$.

METHOD	ARCHITECTURE	TOP-1 ACCURACY	TOP-5 ACCURACY
BASELINE	RESNET50	77.1	93.63
PADAIN	RESNET50	77.7	93.93
BASELINE	RESNET101	78.13	93.71
PADAIN	RESNET101	78.8	94.35
BASELINE	RESNET152	78.31	94.06
PADAIN	RESNET152	79.13	94.64

300 epochs, and use standard augmentations of resizing to 256×256 and applying a random crop of 224×224 and then applying a random horizontal flip. The learning rate is initiated to 0.1 for ResNet50, ResNet101, and ResNet152 after which it is reduced by a factor of 10 every 75 epochs. We use an SGD with Momentum optimizer and the batch size, weight decay and momentum were set to 256, $1e^{-4}$ and 0.9 respectively.

For all experiments, a default value of $p = 0.01$ is used. In Tab. 1 and Tab. 2 we compare, for the different architectures, the result of training the network with pAdaIN and without pAdaIN (Baseline). Other than the use of pAdaIN, which does not add any learnable parameters to the network, the same architecture and training procedure is used. As can be seen, our method outperforms the baseline on the above datasets. The improvement is consistent across networks with a vastly different number of parameters, such as ResNet18 and ResNet50 for CIFAR100 and ResNet50, ResNet101, and ResNet152 for ImageNet. The improvement is also consistent across different model types, such as PyramidNet and ResNet for CIFAR100.

Lastly, we consider the effect of changing p on the overall accuracy. This is done for ResNet18 and ResNet50 model trained on CIFAR100 and ImageNet respectively. As can be seen in Fig. 2, increasing the value of p up to 0.01 results in improved accuracy, after-which accuracy drops.

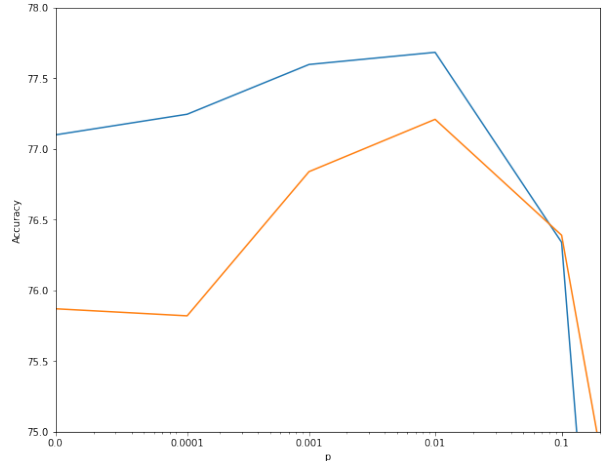


Figure 2. Resnet50 and ResNet18 models trained with pAdaIN for various values of p on ImageNet (blue) and CIFAR100 (orange) respectively. For p values above 0.1 (not shown), accuracy drops significantly below 75% for both ImageNet and CIFAR100.

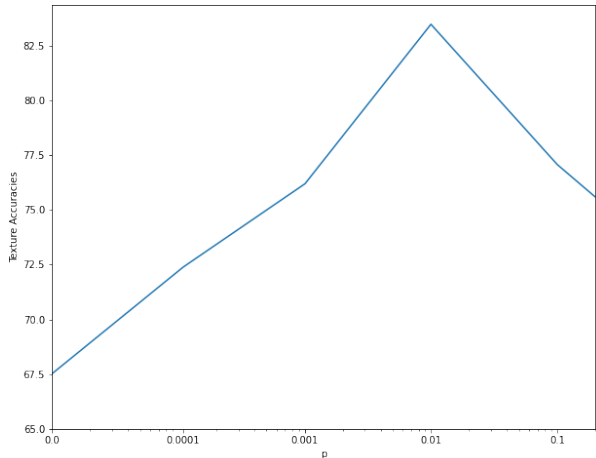


Figure 3. Texture accuracy for ResNet18 trained on CIFAR100 with pAdaIN for various values of p .

4.2. Texture classification

To show stronger feature representation for textures, we evaluate our models using the texture surface dataset [18]. The dataset consists of 64 classes, with a total of 8674 images from three public texture datasets. The dataset is split equally for training and test. Our training procedure consists of freezing the backbone of the trained model, and training a linear classifier on top of the last representation layer of ResNet18 (before the fully connected component) to correctly classify the texture class. A high accuracy indicates that the model captures texture more strongly in its representation layer.

For CIFAR100, we consider the texture accuracy when training with pAdaIN for various values of p . As can be seen in Fig. 3, a critical value of $p = 0.01$ results in the best performing model. As pAdaIN is applied at each layer

with probability p independently, setting p too high can result in an excessive change of statistics, thus resulting in degradation in accuracy.

We note that this coincides in the value of p having the best overall accuracy for CIFAR100, as shown in Fig. 2. Other than moving from $p = 0$ to $p = 0.0001$, an increase (resp. decreasing) in the value p results in an increase (resp. decrease) of both overall accuracy and texture accuracy.

4.3. Multi-domain Generalization

Of a particular interest is the ability of image classifiers to generalize in the settings where the test distribution is shifted compared to the train distribution. In the setting of *domain adaption*, one is given a labeled source data and an unlabeled target data and is asked to generalize well on both the source and target distributions. In the more challenging task of *domain generalization*, the unlabeled source data is not available during training.

To evaluate our method, we consider the PACS dataset [22], which consists of four domains: photo, art, cartoon, and sketch. We follow the multi-source evaluation protocol of [4], in training on three out of the four domains and evaluating on the fourth domain. In our comparison, we consider the latest domain generalization methods and report the accuracy as reported in the relevant paper. For the baseline method comparison, we simply train a network on the source data, without further modifications. Our models are trained with SGD, over 30 epochs, batch size 128. The learning rate is set to 0.001. For the latest domain generalization method, RSC [19], we also independently run the method using the open-source implementation as published by the authors, using the default configuration¹.

Tab. 3 shows the results of our method against that of baseline methods. As can be seen, when trained with pAdaIN, our method, on average, beats all baseline methods on both ResNet18 and ResNet50, except when considered against the reported values of RSC [19]. We note that our method outperforms our independently reproduced results of RSC, which follows the official open source implementation.

4.4. Robustness Towards Corruptions

Convolutional neural networks tend to be sensitive to small perturbations [7]. These small perturbations affect the statistics of the representation layers of the network. It is thus plausible that a model taught to be insensitive to statistical shifts on the feature space, such as our method, would be more robust towards corruptions. To test this hypothesis, we evaluate our method against ImageNet-C and Cifar-100-C [7], corrupted versions of ImageNet and CIFAR100.

First, we consider a ResNet50 model trained on ImageNet with or without pAdaIN. As can be seen in Tab. 4, our

method improves upon the baseline method trained without pAdaIN (with $p = 0.01$). Next, we consider pAdaIN in conjunction with the current state of the art - AugMix [14]. As can be seen, combining pAdaIN with Augmix exceeds Augmix and is thus state of the art. For reference, average test error for additional methods designed for corruption are reported in Tab. 5. Here we note that our smallest improvement is for the noise, blur, pixelated and JPEG corruptions as these preserve the global statistics and have a tendency to modify the fine details. Conversely, weather and contrast corruptions preserve texture and we therefore see an overall greater improvement for these categories.

4.5. Ablation Analysis

We further evaluate different variants of pAdaIN. We consider a ResNet18 network trained on CIFAR100, as described in Sec. 4.1.

In Tab. 6 we consider the effect of using pAdaIN on specific blocks of the ResNet18 network. As can be seen, the effect of pAdaIN is most prominent when applied at the deeper blocks of the network, specifically at blocks 3 and 4.

Next, we wish to understand the importance of permuting the statistics, that is, using the statistics of the feature representation from natural images. Instead of swapping the statistics between feature representations of images, we swap the statistics of an image’s feature representation with random statistics sampled from a normal distribution with zero mean and unit variance. We set the probability for this to happen at $p = 0.01$, as in the default pAdaIN setting. We observed that as the model converged to minimal loss on the training set, the validation performance was very unstable, both in terms of loss and test accuracy. The overall accuracy is 57.3, which is significantly lower. We believe this is due to the distribution shift from the statistics of natural images, happening with probability p .

5. Conclusions

While neural network image classifiers are extremely powerful, they still incorporate some amount of reliance on global image statistics that are easy to manipulate without changing the image semantics. In this work, we make use of the normalization mechanism to remove the reliance on this bias. The method is probabilistic and has a parameter p that controls the tradeoff between training on deliberately mismatched image statistics and employing the matching global statistics. Naturally, there is exploitable information in these statistics that can help in image recognition benchmarks.

Since the texture is often defined as image statistics, and since previous work has focused on removing the bias toward texture, it is important to make the distinction between texture and global image statistics. As our motivating example shows, texture patterns are largely invariant to changes

¹See <https://github.com/DeLightCMU/RSC>

Table 3. Results on multi-source domain generalization on the PACS dataset. The top part of the table shows the results for ResNet18 and the bottom part shows the result for ResNet50 architecture. Highlighted are the best scores per category. For this purpose, we consider RSC [19] reproduced scores and not the reported ones (see Sec. 4.3 for details).

Method	Architecture	photo	art	cartoon	sketch	average
Baseline [4]	ResNet18	95.98	77.87	74.86	70.17	79.72
D-SAM [9]	ResNet18	95.30	77.33	72.43	77.83	80.72
JiGen [4]	ResNet18	96.03	79.42	75.25	71.35	80.51
MASF [8]	ResNet18	94.99	80.29	77.17	71.69	81.03
Epi-FCR [23]	ResNet18	93.90	82.10	77.00	73.00	81.50
MetaReg [3]	ResNet18	95.50	83.70	77.20	70.30	81.70
InfoDrop [26]	ResNet18	96.11	80.27	76.54	76.38	82.32
RSC [19] (reported)	ResNet18	95.99	83.43	80.31	80.85	85.15
RSC [19] (reproduced)	ResNet18	94.10	78.90	76.88	76.81	81.67
pAdaIN (ours)	ResNet18	96.29	81.74	76.91	75.13	82.51
Baseline [4]	ResNet50	97.66	86.20	78.70	70.63	83.29
MASF [8]	ResNet50	95.01	82.89	80.49	72.29	82.67
MetaReg [3]	ResNet50	97.60	87.20	79.20	70.30	83.60
RSC [19] (reported)	ResNet50	97.92	87.89	82.16	83.35	87.83
RSC [19] (reproduced)	ResNet50	93.72	81.38	80.14	82.31	84.38
pAdaIN (ours)	ResNet50	97.17	85.82	81.06	77.37	85.36

Table 4. Clean Top-1 Error (E), Mean Corruption Error (mCE) and Corruption Error values of different corruptions. First we consider an ImageNet trained ResNet50 model with or without pAdaIN, evaluated on IMAGENET-C. Second, we consider DenseNet and ResNext models trained on CIFAR-100 either with Augmix alone or together with pAdaIN and evaluated on CIFAR-100-C. Lower is better.

Dataset	Network	Architecture	E	mCE	Noise			Blur				Weather				Digital			
					Gauss.	Shot	Impulse	Defocus	Glass	Motion	Zoom	Snow	Frost	Fog	Bright	Contrast	Elastic	Pixel	JPEG
ImageNet-C	Baseline	ResNet50	23.9	76.7	80	82	83	75	89	78	80	78	75	66	57	71	85	77	77
ImageNet-C	pAdaIN	ResNet50	22.3	72.8	78	79	81	70	87	74	76	74	71	64	55	65	82	66	71
Cifar-100-C	Augmix [14]	DenseNet	24.2	38.9	60	51	41	27	55	31	29	36	39	35	28	37	33	39	41
Cifar-100-C	Augmix+pAdaIN	DenseNet	22.3	37.6	59	50	40	26	54	30	28	35	38	33	26	36	32	36	40
Cifar-100-C	Augmix [14]	ResNext	21.0	34.4	56	48	32	23	49	27	25	32	35	32	24	32	30	34	37
Cifar-100-C	Augmix+pAdaIN	ResNext	17.3	31.6	58	48	24	20	54	23	21	28	30	25	19	27	27	33	36

in global image statistics, even if these occur simultaneously across multiple encoding channels.

Indeed, contrary to the results of the methods for correcting texture bias, we demonstrate that the increase in

classification performance goes hand in hand with the increase in classification capabilities on image texture datasets. We do not believe this to be a misinterpretation by previous work, since we tested performance of selected texture bias

Table 5. Classification error in comparison to state of the art baselines on CIFAR-100-C for the ResNext [30] and DenseNet [16] architectures. pAdaIN in conjunction with Augmix [14] exceeds the state of the art. Baseline indicates a network trained on CIFAR-100 without any modifications.

	Baseline	Cutout [6]	Mixup [31]	CutMix [31]	Auto-Augment [5]	Adversarial Training [24]	Augmix [14]	pAdaIN+ Augmix
DenseNet	59.3	59.6	55.4	59.2	53.9	55.2	38.9	37.6
ResNext	53.4	54.6	51.4	54.1	51.3	54.4	34.4	31.6

Table 6. pAdaIN on different blocks of a ResNet18 trained on CIFAR100

LAYERS	NONE	1	2	3	1+2+3	4	3+4	ALL
ACCURACY	76.13	75.9	76.1	76.5	76.4	77.5	78.1	77.82

removal methods on texture datasets and observed a decrease in performance. We, therefore, believe that the two effects are distinct.

Despite this distinctiveness, both the texture bias removal methods and our method demonstrate an increase in the recognition capabilities in shifted domains, including various effects and corrupted images.

References

- [1] Anonymous. Domain generalization with mixstyle. In *Submitted to International Conference on Learning Representations*, 2021. under review. [2](#)
- [2] Jimmy Lei Ba, Jamie Ryan Kiros, and Geoffrey E Hinton. Layer normalization. *arXiv preprint arXiv:1607.06450*, 2016. [2](#)
- [3] Yogesh Balaji, Swami Sankaranarayanan, and Rama Chellappa. Metareg: Towards domain generalization using meta-regularization. In *Advances in Neural Information Processing Systems*, pages 998–1008, 2018. [6](#)
- [4] Fabio M Carlucci, Antonio D’Innocente, Silvia Bucci, Barbara Caputo, and Tatiana Tommasi. Domain generalization by solving jigsaw puzzles. In *Proceedings of the IEEE Conference on Computer Vision and Pattern Recognition*, pages 2229–2238, 2019. [2](#), [5](#), [6](#)
- [5] Ekin D Cubuk, Barret Zoph, Dandelion Mane, Vijay Vasudevan, and Quoc V Le. Autoaugment: Learning augmentation policies from data. *arXiv preprint arXiv:1805.09501*, 2018. [6](#)
- [6] Terrance DeVries and Graham W Taylor. Improved regularization of convolutional neural networks with cutout. *arXiv preprint arXiv:1708.04552*, 2017. [6](#)
- [7] Samuel Dodge and Lina Karam. A study and comparison of human and deep learning recognition performance under visual distortions. In *2017 26th international conference on computer communication and networks (ICCCN)*, pages 1–7. IEEE, 2017. [5](#)
- [8] Qi Dou, Daniel Coelho de Castro, Konstantinos Kamnitsas, and Ben Glocker. Domain generalization via model-agnostic learning of semantic features. In *Advances in Neural Information Processing Systems*, pages 6450–6461, 2019. [6](#)
- [9] Antonio D’Innocente and Barbara Caputo. Domain generalization with domain-specific aggregation modules. In *German Conference on Pattern Recognition*, pages 187–198. Springer, 2018. [6](#)
- [10] Leon Gatys, Alexander S Ecker, and Matthias Bethge. Texture synthesis using convolutional neural networks. In *Advances in neural information processing systems*, pages 262–270, 2015. [1](#), [2](#), [3](#)
- [11] Robert Geirhos, Patricia Rubisch, Claudio Michaelis, Matthias Bethge, Felix A Wichmann, and Wieland Brendel. Imagenet-trained cnns are biased towards texture; increasing shape bias improves accuracy and robustness. *arXiv preprint arXiv:1811.12231*, 2018. [1](#), [2](#)
- [12] Dongyoon Han, Jiwhan Kim, and Junmo Kim. Deep pyramidal residual networks. In *Proceedings of the IEEE conference on computer vision and pattern recognition*, pages 5927–5935, 2017. [3](#)
- [13] Kaiming He, Xiangyu Zhang, Shaoqing Ren, and Jian Sun. Deep residual learning for image recognition. In *Proceedings of the IEEE conference on computer vision and pattern recognition*, pages 770–778, 2016. [3](#)
- [14] Dan Hendrycks, Norman Mu, Ekin D Cubuk, Barret Zoph, Justin Gilmer, and Balaji Lakshminarayanan. Augmix: A simple data processing method to improve robustness and uncertainty. *arXiv preprint arXiv:1912.02781*, 2019. [5](#), [6](#)
- [15] Katherine L Hermann and Simon Kornblith. Exploring the origins and prevalence of texture bias in convolutional neural networks. *arXiv preprint arXiv:1911.09071*, 2019. [2](#)
- [16] Gao Huang, Zhuang Liu, Laurens Van Der Maaten, and Kilian Q Weinberger. Densely connected convolutional networks. In *Proceedings of the IEEE conference on computer vision and pattern recognition*, pages 4700–4708, 2017. [6](#)
- [17] Xun Huang and Serge Belongie. Arbitrary style transfer in real-time with adaptive instance normalization. In *Proceedings of the IEEE International Conference on Computer Vision*, pages 1501–1510, 2017. [2](#), [3](#)
- [18] Yibin Huang, Congying Qiu, Xiaonan Wang, Shijun Wang, and Kui Yuan. A compact convolutional neural network for surface defect inspection. *Sensors*, 20(7):1974, 2020. [4](#)
- [19] Zeyi Huang, Haohan Wang, Eric P Xing, and Dong Huang. Self-challenging improves cross-domain generalization. *arXiv preprint arXiv:2007.02454*, 2020. [5](#), [6](#)
- [20] Sergey Ioffe and Christian Szegedy. Batch normalization: Accelerating deep network training by reducing internal covariate shift. *arXiv preprint arXiv:1502.03167*, 2015. [2](#)
- [21] Jonathan Krause, Michael Stark, Jia Deng, and Li Fei-Fei. 3d object representations for fine-grained categorization. In *4th International IEEE Workshop on 3D Representation and Recognition (3dRR-13)*, Sydney, Australia, 2013. [2](#)
- [22] Da Li, Yongxin Yang, Yi-Zhe Song, and Timothy Hospedales. Deeper, broader and artier domain generalization. In *International Conference on Computer Vision*, 2017. [5](#)
- [23] Da Li, Jianshu Zhang, Yongxin Yang, Cong Liu, Yi-Zhe Song, and Timothy M Hospedales. Episodic training for domain generalization. In *Proceedings of the IEEE International Conference on Computer Vision*, pages 1446–1455, 2019. [6](#)
- [24] Aleksander Madry, Aleksandar Makelov, Ludwig Schmidt, Dimitris Tsipras, and Adrian Vladu. Towards deep learning models resistant to adversarial attacks. *arXiv preprint arXiv:1706.06083*, 2017. [6](#)

- [25] T. Sakai, M. Nagao, and Takeo Kanade. Picture structure and its processing – the case of human-face photographs. In *Proceedings of Joint Conference of Electrical Engineers of Japan*, October 1971. 1
- [26] Baifeng Shi, Dinghuai Zhang, Qi Dai, Zhanxing Zhu, Yadong Mu, and Jingdong Wang. Informative dropout for robust representation learning: A shape-bias perspective. *arXiv preprint arXiv:2008.04254*, 2020. 2, 6
- [27] Dmitry Ulyanov, Andrea Vedaldi, and Victor Lempitsky. Instance normalization: The missing ingredient for fast stylization. *arXiv preprint arXiv:1607.08022*, 2016. 2
- [28] Haohan Wang, Songwei Ge, Zachary Lipton, and Eric P Xing. Learning robust global representations by penalizing local predictive power. In *Advances in Neural Information Processing Systems*, pages 10506–10518, 2019. 2
- [29] Yuxin Wu and Kaiming He. Group normalization. In *Proceedings of the European conference on computer vision (ECCV)*, pages 3–19, 2018. 2
- [30] Saining Xie, Ross Girshick, Piotr Dollár, Zhuowen Tu, and Kaiming He. Aggregated residual transformations for deep neural networks. In *Proceedings of the IEEE conference on computer vision and pattern recognition*, pages 1492–1500, 2017. 6
- [31] Sangdoo Yun, Dongyoon Han, Seong Joon Oh, Sanghyuk Chun, Junsuk Choe, and Youngjoon Yoo. Cutmix: Regularization strategy to train strong classifiers with localizable features. In *Proceedings of the IEEE International Conference on Computer Vision*, pages 6023–6032, 2019. 6
- [32] Hongyi Zhang, Moustapha Cisse, Yann N Dauphin, and David Lopez-Paz. mixup: Beyond empirical risk minimization. *arXiv preprint arXiv:1710.09412*, 2017. 2
- [33] Tianyuan Zhang and Zhanxing Zhu. Interpreting adversarially trained convolutional neural networks. *arXiv preprint arXiv:1905.09797*, 2019. 2